Utilizing magnetization and spin in thermoelectric applications

Sarah J. Watzman,* Takashi Kikkawa, Brian Skinner, and Ken-ichi Uchida

The combined use of heat, charge, and spin transport gives rise to new or deeply altered thermoelectric properties from those found in conventional, nonmagnetic thermoelectric transport; these phenomena include the magneto-Seebeck, Nernst, magnon drag, and spin Seebeck effects. Here, we explore both electron-driven and magnon-driven magneto-thermoelectric effects stemming from different origins depending on if the effect is longitudinal, where the electric field and thermal gradient are collinear, or transverse, where the electric field and thermal gradient are orthogonal. We consider both a Lorentz force acting on charge carriers in nonmagnetic conductors and the spin–orbit interaction acting on spin-polarized electrons in magnetic materials. Both intrinsic and extrinsic sources of skew forces on electrons or anomalous velocities offer promising avenues for generating new functionalities and applications in the burgeoning field of magneto-thermoelectrics and transverse thermoelectrics. Adding magnetism as a design degree of freedom offers more candidate classes of materials, such as topological, metallic, and amorphous materials, for consideration in the field of thermoelectrics.

Introduction: Magneto-thermoelectric phenomena and their origins

The field of thermoelectrics began with the initial discovery of the Seebeck effect by T.J. Seebeck in the early 1820s.[1] Conventional thermoelectric devices require alternating pairs of *n*-type and *p*-type semiconductors connected electrically in series and thermally in parallel to generate an output voltage from an input heat flux. Much research in the field has focused on increasing zT, the dimensionless figure of merit, although recent progress in the field has not brought significant enhancements to make conventional thermoelectric devices and materials competitive for consumer applications.[2] However, the first observation of the spin Seebeck effect (SSE) in 2008[3] and the experimental discovery of Weyl semimetals (WSMs) in 2015[4–7] have brought resurgence in interest in using magnetization and spin in thermoelectric applications to enhance thermal-to-electrical energy conversion and offer geometrical freedom in device design. The Nernst effect, first discovered by Walther Nernst and Albert von Ettingshausen in elemental bismuth in 1886,[8] employs a transverse geometry in which an applied heat flux and orthogonal external magnetic field generate a Lorentz force, accelerating charge carriers in a mutually perpendicular direction to generate a transverse electric field. Although a plethora of magneto-thermoelectric effects exist, here we focus on the magneto-Seebeck effect, magnon-drag thermopower, Nernst effect, and SSE-induced inverse spin Hall effect (ISHE), as these phenomena are representative of both electron-driven and magnon-driven longitudinal and transverse magneto-thermoelectric effects, as shown in **Figure 1**. We have chosen these four representative transport phenomena to demonstrate to readers both the geometrical opportunities (longitudinal and transverse) and the opportunities in origin of transport phenomena (electron-driven and magnon-driven) offered by magneto-thermoelectrics, which are not found in the field of conventional thermoelectrics.

Magneto-thermoelectric transport phenomena

In Figure 1, the thermoelectric effects discussed in this article are classified in terms of energy carriers and configurations. In both magnetic and nonmagnetic materials and their hybrid systems, a wide variety of transport phenomena occur, but in this article, we focus on the magneto-Seebeck effect, Nernst effect, magnon-drag (MD) thermopower, and SSE-induced ISHE. The magneto-thermoelectric transport phenomena are

Sarah J. Watzman, Department of Mechanical and Materials Engineering, University of Cincinnati, Cincinnati, USA; watzmasj@ucmail.uc.edu
Takashi Kikkawa, Advanced Science Research Center, Japan Atomic Energy Agency, Tokai, Japan; kikkawa.takashi@jaea.go.jp
Brian Skinner, Department of Physics, The Ohio State University, Columbus, USA; skinner.352@osu.edu
Ken-ichi Uchida, Research Center for Magnetic and Spintronic Materials, National Institute for Materials Science, Tsukuba, Japan; Department of Advanced Materials Science, The University of Tokyo, Kashiwa, Japan; UCHIDA.Kenichi@nims.go.jp
*Corresponding author
doi:10.1557/s43577-025-00941-8

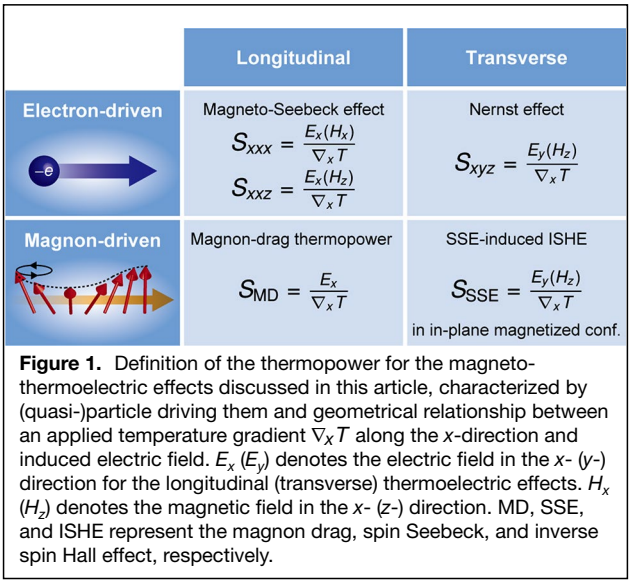

Figure 1. Definition of the thermopower for the magneto-thermoelectric effects discussed in this article, characterized by (quasi-)particle driving them and geometrical relationship between an applied temperature gradient $\nabla_x T$ along the *x*-direction and induced electric field. E_x (E_y) denotes the electric field in the *x*- (*y*-) direction for the longitudinal (transverse) thermoelectric effects. H_x (H_z) denotes the magnetic field in the *x*- (*z*-) direction. MD, SSE, and ISHE represent the magnon drag, spin Seebeck, and inverse spin Hall effect, respectively.

thermoelectric effects that occur depending on the external magnetic field or the direction of spontaneous magnetization; they are categorized into longitudinal effects, in which an electric field is generated in a direction parallel to an input temperature gradient, and transverse effects, in which an electric field is generated in a direction perpendicular to the temperature gradient.

The most fundamental phenomenon of the electron-driven longitudinal magneto-thermoelectric effects is the magneto-Seebeck effect. This is a phenomenon in which the Seebeck coefficient changes depending on the magnetic field, and the behavior differs depending on whether the magnetic field is parallel or perpendicular to the temperature gradient (Figure 1, and **Figure 2**a).[9–11] In magnetic materials with spontaneous magnetization, the Seebeck coefficient changes anisotropically with respect to the magnetization direction; this phenomenon is thus called the anisotropic magneto-Seebeck effect. In contrast, the electron-driven transverse magneto-thermoelectric effect is called the Nernst effect. Its popularity has increased in condensed-matter physics in recent years, following the development of topological materials science and spin caloritronics. In the ordinary (anomalous) Nernst effect, when an external magnetic field (spontaneous magnetization) is oriented in the *z*-direction, an electric field is generated in the *y*-direction when a temperature gradient is applied in the *x*-direction (Figures 1 and 2b).[12–15]

However, the magneto-thermoelectric effects are caused not only by the transport of conduction electrons/holes but also by the transport of quasiparticles such as magnons (i.e., collective excitations of localized magnetic moments). The phenomenon in which the Seebeck coefficient changes as electrons or holes receive momentum from phonons is known as phonon drag, and a similar phenomenon occurring with magnons is called magnon drag.[17–19] The magnon drag is classified as a longitudinal magneto-thermoelectric effect because it modulates the Seebeck coefficient through magnon transport (Figure 1). SSE-induced ISHE is classified as a magnon-driven transverse magneto-thermoelectric effect in this article. This is because, while ISHE is a phenomenon in which a conduction-electron spin current is converted into an electric field in a nonmagnetic conductor, SSE generates a magnon spin current in a magnetic material. The symmetry of the thermoelectric conversion by SSE-induced ISHE is similar to that by the Nernst effect, but SSE-induced ISHE works only when the magnetization direction of the magnetic material is oriented within the junction interface between the magnetic material and nonmagnetic conductor (Figures 1 and 2c).[16,20–22]

Magnetic and spin origins of magneto-thermoelectric effects

The origins of the electron-driven magneto-thermoelectric effects are the Lorentz force acting on charge carriers in

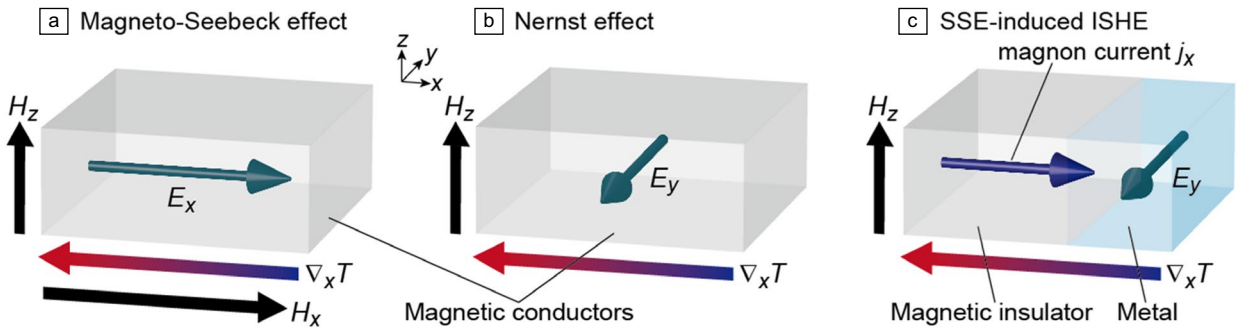

Figure 2. Schematics of the (a) magneto-Seebeck effect, (b) Nernst effect, and (c) spin Seebeck effect (SSE)-induced inverse spin Hall effect (ISHE). Note that the direction of the generated electric fields E_x and E_y depends on the sign of the magneto-Seebeck thermopowers S_{xxx} and S_{xxz} for (a), the Nernst thermopower S_{xyz} for (b), and the SSE thermopower S_{SSE} (which is determined by the sign of the magnon polarization of the magnetic layer and the spin-Hall angle of the metallic layer[16]) for (c). The external magnetic field (H_x or H_z) orients the magnetization **M** in the magnetic layers parallel to the field direction.

nonmagnetic conductors and the spin–orbit interaction acting on spin-polarized electrons in magnetic materials. When the applied temperature gradient and external magnetic field are orthogonal, the Lorentz force bends the trajectory of charge carriers driven by the temperature gradient, resulting in the ordinary Nernst effect in nonmagnetic conductors. As a second-order effect of the magnetic field, the longitudinal transport properties also change, resulting in the magneto-Seebeck effect, which is a thermoelectric analogue of the magnetoresistance. In magnetic materials, the spin–orbit interaction anisotropically changes the hybridization of the electronic bands, resulting in the anisotropic magneto-Seebeck effect.[11] The origin of the anomalous Nernst effect (ANE) is also the spin–orbit interaction, but, in a similar manner to the anomalous Hall effect, it can be classified into an intrinsic mechanism that originates in the electronic band structure and an extrinsic mechanism that originates in spin-dependent impurity scattering. The recent trend is to search for materials that exhibit large ANE due to intrinsic mechanisms; in various topological materials, large anomalous Nernst coefficients and transverse thermoelectric conductivities have been observed because of the large Berry curvature near the Fermi energy owing to the specific band structures, including Weyl points, nodal lines, webs, and planes.[12–15] The same is true for the Onsager reciprocal of the previously discussed phenomena.

The origins of the magnon-driven magneto-thermoelectric effects are fundamentally different from those of the electron-driven effects. Magnons do not carry a charge, but they modulate the thermoelectric conversion properties of electrons via electron–magnon scattering and a spin-motive force, which is an electric field induced by the energy transfer between conduction-electron spins and magnetic moments; this is the magnon-drag thermopower.[17] Magnon-drag thermopower can persist even in a paramagnetic state as short-range spin fluctuations.[18,19] On the other hand, SSE is a phenomenon that directly generates a magnon spin current from a temperature gradient in a magnetic material. The transverse thermopower induced by SSE is generated through three key steps: (1) an applied temperature gradient in the magnetic layer induces a flow of magnons (i.e., a magnon spin current), which (2) at the interface with the metallic contact is converted into a conduction-electron spin current via the interfacial exchange interaction and (3) is subsequently detected as a transverse voltage via ISHE.[16,20–22]

Review of material advances in magneto-thermoelectrics

Anomalous Nernst effect (ANE)

Topological materials

Topological materials have attracted significant attention in the field of solid-state physics since their first experimental confirmation[4–7] and are of particular interest in magneto-thermoelectrics due to the ultrahigh mobility found in their Dirac bands.[23,24] In particular, the unique features of WSMs, such as bulk Weyl nodes[23,24] and surface Fermi arcs,[25] were expected to have signatures in magneto-thermoelectric transport beyond those from classical electronic contributions. Specifically, Berry curvature was expected to contribute to an ANE even in the absence of ferromagnetism.[26,27] The first topological material in which this was observed was Cd_3As_2, a Dirac semimetal, where the anomalous Nernst signal increases significantly above ~50 K; here, the ANE is linked to topological protection as the transport relaxation time increases in the same temperature range.[28] Berry curvature was determined as the source of the large ANE.[28] due to the external magnetic field breaking time-reversal symmetry and thus lifting the degeneracy of the Dirac nodes, splitting them into Weyl nodes. NbP is the first WSM in which ANE was observed, with ANE exceeding the ordinary Nernst effect in fields of magnitude less than ~2 T and an unsaturating transverse thermopower S_{xyz} up to 9 T with a maximum observed value of ~800 μV K^{-1} at 109 K.[29] Both the Seebeck coefficient and S_{xyz} were observed to have maximum values in similar temperature ranges, and this behavior was attributed to the temperature-dependent motion of the chemical potential that got pinned at the energy of the Weyl points due to the charge neutrality condition arising from a zero density of states at the energy of the Weyl points when no trivial pockets contribute to transport.[29] Although no magneto-Seebeck effect was observed in single-crystalline NbP,[29] a large magneto-Seebeck effect was observed in polycrystalline NbP over a broad temperature range; S_{xxz} was also observed to maximize over a similar temperature range as S_{xyz},[30,31] which is unique to this class of materials. The differences in magneto-thermoelectric transport data among these samples of NbP was later attributed to the sensitivity of WSMs to slight changes in composition, suggesting that doping could be used as a tuning mechanism for magneto-thermoelectric effects in not only NbP but topological materials in general.[31] Interestingly, both S_{xxz} and S_{xyz} being maintained near their maximal values over broad temperature ranges are currently theoretically predicted to be a trait specific to compensated or nearly compensated Type I WSMs, where their Dirac bands are symmetric about an energy axis in k-space.[32] Recent work in WTe_2, a Type II WSM whose Dirac bands are tilted in k-space, supports this claim as its S_{xyz} is near 8000 μV K^{-1} at 9 T near ~10–15 K but quickly drops near zero by ~30 K.[33]

Although exciting, reported values of ANE in the aforementioned materials required large, externally applied magnetic fields, making these materials potentially incompatible with conventional thermal energy-conversion applications. However, WSMs that break time-reversal symmetry are expected to have a net Berry curvature, which can act like a magnetic field while being intrinsic to a material's band structure.[24,26] Recent work in ferromagnetic WSMs, such as Co_2MnGa, indicates that Berry curvature can indeed lead to a giant ANE, beyond that expected from intrinsic magnetization alone.[12,13] ANE was also observed in $Co_3Sn_2S_2$, a hard ferromagnet, at zero-field,[34,35] and the Nernst conductivity's scaling relation with the material's magnetization determined that Berry curvature was the dominant mechanism behind the

large ANE.[35,36] Recent attention has turned to antiferromagnetic WSMs, which offer further potential in device applications as they do not have the stray magnetic fields associated with ferromagnetic materials.[37] $YbMnBi_2$ is a time-reversal symmetry breaking Type II WSM, and it is a canted antiferromagnet.[38] In $YbMnBi_2$, the ANE is highly anisotropic, in part due to the highly anisotropic band structure and in part due to the directionality associated with spin canting. The sign of the Berry curvature, and therefore the sign of the anomalous Hall conductivity, is determined by the direction of the spin canting, which can be toggled by a weak external magnetic field applied in the canting direction. $YbMnBi_2$ thus offers promise as a switchable transverse thermoelectric.[39]

Permanent magnets

The appearance of giant ANE is not an exclusive feature of topological materials. In 2019, $SmCo_5$-type permanent magnets were discovered, which are mass-produced and used in practical applications, and they exhibit large ANE.[40] The anomalous Nernst thermopower, S_{ANE} (a subset of S_{xyz} from Figure 1 corresponding specifically to the ANE) of $SmCo_5$ exceeds 3.5 μV K^{-1} at room temperature, monotonically increases with increasing temperature, and reaches >5.5 μV K^{-1} at $T > 550$ K.[41] Although these values are smaller than S_{ANE} of Co_2MnGa, the ratio of the electrical conductivity σ to the thermal conductivity κ of the $SmCo_5$-type magnets is larger than that of Co_2MnGa. Thus, the figure of merit for ANE in these materials is comparable. The transverse thermoelectric conductivity of the $SmCo_5$-type magnet at room temperature (4.6 A K^{-1} m^{-1}) was estimated to be much larger than that of Co_2MnGa (2.4–3.0 A K^{-1} m^{-1}). The $SmCo_5$-type magnets are known as permanent magnets with excellent temperature stability. Their coercive force is extremely large, and the remanent magnetization remains finite up to $T > 700$ K. Therefore, the $SmCo_5$-type magnets enable the zero-field operation of large ANE and can be regarded as top-class ANE materials. Interestingly, $Nd_2Fe_{14}B$-type magnets, which have the largest maximum energy product $(BH)_{max}$ and are the most widely used permanent magnets in society, show negative S_{ANE}, although $|S_{ANE}|$ is small.[40] It has been demonstrated that by alternately stacking the $SmCo_5$-type magnets with $S_{ANE} > 0$ and the $Nd_2Fe_{14}B$-type magnets with $S_{ANE} < 0$ and connecting them in series, it is possible to construct an anomalous Nernst thermopile module that operates in the absence of a magnetic field, in which all the magnets contribute to the total output power.[42] This was demonstrated in the magnetic-field-free ANE-driven power generation up to 177 μW around room temperature at a temperature difference of 75 K, leading to the record-high power density of 65 μW cm^{-2} due to ANE.

ANE in permanent magnets has been investigated mainly using bulk materials. However, magnetic materials having large coercivity and remanent magnetization are useful also for ANE-based thin-film devices, which are developed toward future applications as heat flux sensors.[43] An ANE-based heat flux sensor has a thermopile structure comprising two different thin wire-shaped materials arranged alternately and connected in series, where the temperature gradient is in the thickness direction and the magnetization is in the width direction of the wires. This configuration enables the construction of heat flux sensors with low thermal resistance. Due to the large demagnetization field in the thin wires, the magnetization has to be aligned in the hard axis.[44,45] Thus, materials development is also being carried out to overcome this issue, and promising materials such as $Co_3Sn_2S_2$-based alloys[46] and amorphous Sm-Co-based alloys,[47] described next have been reported. Note that the performance of heat flux sensors is determined by the open-circuit voltage per unit heat flux, and the figure of merit is not a good indicator for this application.

Amorphous materials

While most of the ANE studies to date have been conducted using crystalline materials, amorphous magnetic materials are also promising for applications of ANE because they can be mass-produced inexpensively and have mechanical flexibility. The amorphous structure is also effective in reducing lattice thermal conductivity. In 2022, amorphous Sm-Co-based alloy thin films were developed that can be deposited on any substrate, including flexible polymers and glass, and that exhibit large in-plane coercivity and remanent magnetization.[47] These amorphous alloy films can be used to construct flexible, ultrathin ANE devices that operate without magnetic fields, which are suitable for heat-flux sensing applications. However, S_{ANE} of the amorphous Sm-Co-based alloys remains small: S_{ANE} ~1–1.5 μV K^{-1}. To overcome this situation, Gautam et al. have demonstrated that by applying nanostructure engineering to Fe-based amorphous alloys called Nanomet, the S_{ANE} and ANE power factor are increased by 70% and 200%, respectively, while maintaining the mechanical flexibility and average composition of the alloys.[48] This is exemplified in **Figure 3**b.[49–53] S_{ANE} of the nanostructure-engineered Nanomet ribbon, as shown in Figure 3a, was estimated to be 3.7 μV K^{-1} at room temperature, which is comparable to the values for single-crystalline and polycrystalline topological magnets. It has been shown that the increase in S_{ANE} is due to Cu nanoclustering in the Fe-based amorphous alloys, but the microscopic origin is still unclear. Nevertheless, this study clearly shows that, in addition to the electronic structure and composition of materials, nanostructure engineering is important for improving the thermoelectric performance of ANE. It is also possible to create amorphous magnetic metal ribbons with finite coercivity and remanent magnetization through nanostructure engineering; the zero-field operation of ANE has been demonstrated using such materials.[54]

ANE in amorphous materials is interesting from the viewpoints of not only applications but also physics. The Berry curvature contribution to the transverse transport phenomena, which has been confirmed through research on ANE in topological materials, cannot be defined exactly in amorphous alloys that do not have long-range crystalline order. However, experiments using amorphous Fe-Sn alloys show

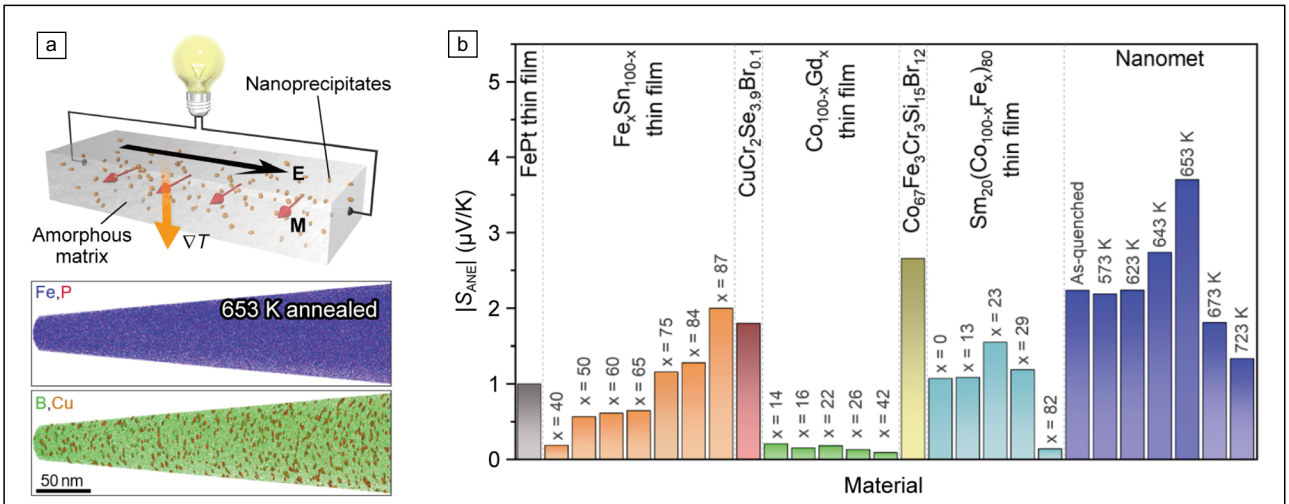

Figure 3. (a) Schematic of anomalous Nernst effect (ANE) in an amorphous magnetic material with nanoprecipitates/cluster and elemental maps of Fe (blue), P (red), B (green), and Cu (orange) for the Nanomet ribbon post-annealed at 653 K, measured by atom probe tomography. (b) Comparison of the absolute values of the ANE thermopower, S_{ANE}, at room temperature for various amorphous magnetic alloys. This figure is reconstructed from Reference 48 licensed under a Creative Commons Attribution 4.0 International License. The data for other materials in (b) are obtained from References 47, 49–53, 55.

that the short-range crystalline order of Kagome-lattice fragments can induce the Berry curvature contribution to ANE and the anomalous Hall effect.[55] As exemplified by this work, the studies on the transport phenomena in amorphous alloys and topological materials are related to each other. It is thus expected that the synergistic effect of these materials will lead to further progress in ANE research.

SSE-induced ISHE

The SSE refers to the generation of a spin current, J_s, as a result of a temperature gradient, ∇T, in a magnetic material with a metallic contact (**Figure 4**).[16,20–22] Thus, SSE is often classified as a thermospin effect, not a magneto-thermoelectric effect.[56] However, SSE functions as a thermoelectric convertor when combined with the ISHE, where the spin current in a magnetic material is injected into a nonmagnetic conductor and converted to an electrical current via ISHE,[16,20–22] so here we classify it as one of the magneto-thermoelectric effects. The effect was first discovered in a ferromagnetic metal permalloy in 2008[3] and later has been observed in a wide range of magnetic materials, including magnetic semiconductors, electrically insulating ferro-, ferri-, and antiferro-magnets, as well as two-dimensional (2D) magnetic materials.[16,20–22] The SSE voltage arises when ∇T is applied in a magnetic material, generating a magnon spin current (Figure 4a), which, at the interface with a metal, is converted into a conduction-electron spin current via the interfacial exchange interaction (Figure 4b) and is subsequently detected as a transverse voltage via the ISHE (Figure 4a).[16,20–22]

From a materials perspective, the ferrimagnetic insulator yttrium-iron-garnet (YIG, $Y_3Fe_5O_{12}$) has been central in SSE research due to its exceptionally low magnetic damping, high electrical resistivity, and high Curie temperature (~560 K). These properties make YIG an ideal platform for studying magnon spin currents and understanding their role in SSE. Extensive SSE studies using YIG-based heterostructures, especially with Pt contacts exhibiting strong ISHE, have provided key insights into the SSE mechanisms.[20,21]

A distinctive aspect of SSE is its involvement of thermally excited magnons with relatively high frequencies in the sub-THz to THz range, enabling studies of magnon spin currents induced by gapped antiferromagnetic

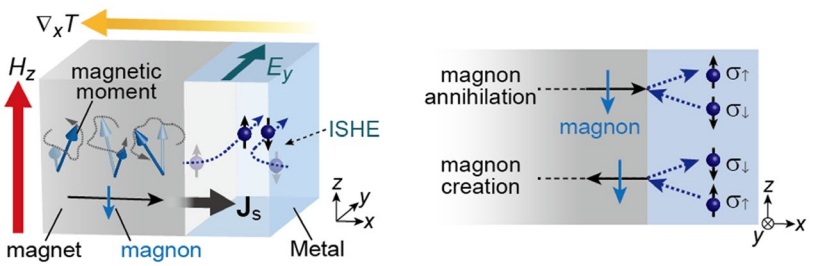

Figure 4. Schematic illustrations of (a) spin Seebeck effect in a magnet/metal junction system and (b) the interfacial magnon–electron-spin scattering due to interfacial spin-exchange interaction. J_s, $\sigma_{\uparrow(\downarrow)}$, E_{ISHE}, ∇T, and H_z denote the spatial direction of the spin current, the up (down) electron spin, the electric field induced by inverse spin Hall effect, the temperature gradient, and the external magnetic field, respectively.

magnon modes. For instance, References 57–60 report the observation of antiferromagnetic SSEs in easy-axis antiferromagnets Cr_2O_3, MnF_2, and α-Fe_2O_3, which host two degenerated antiferromagnetic magnon modes with opposite spin polarization above ~0.1 THz at zero magnetic field. An external magnetic field lifts this degeneracy, creating an imbalance between the two modes, which in turn generates a net magnon spin current. The SSE voltages in these systems exhibit characteristic features reflecting the magnetic-field response of the magnon branches.[57–60] However, their voltage sign remains debated and has been suggested to depend on interfacial details.[60–62] Resolving this issue is a key SSE research challenge.

SSEs in 2D van der Waals magnets represent another promising direction. These materials exhibit spin correlations that differ between in-plane and out-of-plane directions. SSE signals linked to such anisotropies have been studied in $Cr_2Si_2Te_6$ and $Cr_2Ge_2Te_6$.[63] Moreover, SSEs in 2D van der Waals magnets have recently been actively studied in nonlocal configurations,[16] as demonstrated in $MnPS_3$,[64,65] $CrPS_4$,[66] and $CrBr_3$.[67] Another exciting avenue is tuning SSE via stacking order and combinations of 2D materials (e.g., References 68 and 69), which may open new research opportunities.

Magnon-drag effects in metals

While magnon-driven, SSE-induced ISHE requires an interface between a magnetic material and a metallic contact, ferromagnetic metals exhibit magnon transport without the need for an interface. Early work in elemental iron suggested that its Seebeck coefficient was larger than theoretically predicted by diffusion alone and potentially dominated by magnon drag,[70] an advective transport mechanism. Magnons are quasiparticles stemming from the collective excitation of magnetization that carry both linear and spin angular momentum; in the presence of a temperature gradient, heat is transferred to magnons from phonons, and electrons can be pulled through solid materials as the magnon moves through them, as shown in **Figure 5**.[71,72]

Magnon drag was shown to dominate the thermopower of elemental iron and cobalt and contribute to the thermopower of elemental nickel, all of which are transition-metal ferromagnets.[17] A hydrodynamic theory,[73] in which magnons and electrons are treated as interpenetrating fluids, suggests that the magnon drag contribution to thermopower scales with the magnon specific heat, which scales with $T^{3/2}$; electronic diffusion thermopower scales linearly with T,[74] and the sum of the two thermopowers amounts to the total measured thermopower.[17] Interestingly, a microscopic theory based on spin-motive forces[75] gives the same result for magnon-drag thermopower when a Berry phase correction is applied.[76]

Magnon drag is also expected to contribute to the ANE and was experimentally shown to do so in elemental iron.[17] A spin-mixing model was considered, in which independent spin-up and spin-down conduction electron channels exist; each channel was treated separately, as is done for two-carrier transport in semimetals and semiconductors.[77] When the thermopower

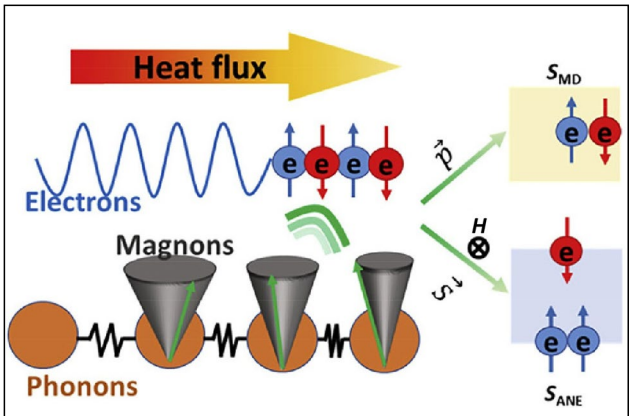

Figure 5. Schematic of magnon drag contributions to thermopower (S_{MD}) and ANE (S_{ANE}). Heat flux is transferred from phonons to magnons in ferromagnets. Magnons carry linear angular moment ($\vec{p}$), which creates S_{MD} when transferred to electrons; magnons also carry spin angular momentum ($\vec{S}$), which creates S_{ANE} when transferred to electrons in materials with large spin–orbit coupling. Figure reproduced from Reference 72 under the terms of the Creative Commons CC-BY license.

contribution to the Nernst coefficient was dominated by magnon-drag thermopower, the anomalous Nernst coefficient was also found to scale with the magnon-drag thermopower, which scales with $T^{3/2}$.[17] More recent work in MnBi suggests that extrinsic contributions from magnons can actually dominate the ANE, where the presence of large spin–orbit coupling leads to an additional spin polarization of conduction electrons in the presence of a thermal gradient, enhancing the transverse voltage (Figure 5).[72]

Nonlinear effects driven by Berry curvature dipole

In the absence of time-reversal symmetry breaking, either by an external magnetic field or by internal magnetic order, transverse linear responses such as the Hall and Nernst effects are forbidden by symmetry. Materials with time-reversal symmetry can still possess finite Berry curvature at different points in momentum space, but the net Berry curvature integrated over the volume of filled electron states must be zero so that the Berry curvature provides no net effect in transverse linear responses.

However, the same constraint does not apply to nonlinear effects, in which a current flows that is proportional to two powers of an applied field. For example, a transverse electrical current can appear in materials possessing time-reversal symmetry so long as this current is proportional to the square of the longitudinal electric field. This effect is dubbed the nonlinear Hall effect,[78] and it has received a number of experimental confirmations in recent years (e.g., References 79 and 80). The idea of the nonlinear Hall effect is that under the influence of an electric field, the volume of filled states shifts in momentum space. If the Berry curvature has a finite dipole moment in the direction of the field, then the shifted Fermi volume has a net Berry curvature even though the equilibrium Fermi volume does not, such that a transverse response is generated under the influence of the electric field.

A similar shift of the Fermi surface can be accomplished by a temperature gradient, which allows for a nonlinear ANE, in which a transverse voltage appears that is proportional to the square of the longitudinal temperature difference.[81–84] The magnitude of the effect is directly proportional to the Berry curvature dipole in the direction of the temperature gradient. Related effects that can be driven by the Berry curvature dipole include an anomalous nonlinear thermal Hall effect, in which a transverse heat current is proportional to the squared longitudinal temperature difference, and an anomalous nonlinear thermoelectric Hall conductivity, in which a transverse voltage arises that is proportional to the product of a longitudinal voltage and a longitudinal temperature difference.[81–84]

To date, there are no published experimental works demonstrating a nonlinear thermoelectric effect driven by the Berry curvature dipole. Yet theoretical work has pointed to a number of candidate materials in which this effect may be detectable, including layered compounds such as bilayer WTe_2,[85] MoS_2,[82] and other transition-metal dichalcogenides;[86] bulk WSMs such as TaAs and $MoTe_2$;[87,88] and the antiferromagnetic semiconductor CuMnAs.[89] Because the magnitude of the Berry curvature dipole can vary sensitively with the chemical potential,[87] achieving precise control over chemical doping or electrical gating may be key for realizing and exploiting these effects. We note that a nonlinear ANE has recently been observed in a superconductor/magnet junction system with broken time-reversal symmetry,[90] and the lock-in-based technique can also be applied to measure nonlinear ANEs arising from the Berry curvature dipole.

Applications for magneto-thermoelectrics

Magneto-thermoelectric figure of merit

The efficiency of conventional thermoelectric conversion increases with the dimensionless figure of merit, zT:

$$zT = \frac{S^2\sigma}{\kappa}T, \tag{1}$$

where S is the Seebeck coefficient and T is the absolute temperature. A dimensionless figure of merit can similarly be defined for thermomagnetic materials based on the magneto-Seebeck (Equations 2 and 3) and Nernst (Equation 4) effects as:

$$(zT)_{xxx} = \frac{S_{xxx}^2\sigma_{xxx}}{\kappa_{xxx}}T \tag{2}$$

$$(zT)_{xxz} = \frac{S_{xxz}^2\sigma_{xxz}}{\kappa_{xxz}}T \tag{3}$$

$$(zT)_{xyz} = \frac{S_{xyz}^2\sigma_{yyz}}{\kappa_{xxz}}T, \tag{4}$$

where $(zT)_{xxx}$, $(zT)_{xxz}$, and $(zT)_{xyz}$ are now functions of both temperature and magnetic field. For the magneto-thermoelectric effects, the electrical conductivity must be taken in the same direction as the induced electric field and the thermal conductivity must be taken in the same direction as the applied heat flux, both in the presence of a magnetic field or magnetization. This implies that in order to fully characterize the figure of merit for a magneto-thermoelectric material, the magneto-electrical conductivity and magneto-thermal conductivity must also be measured in addition to the magneto-thermoelectric effect itself. Ideally, these would be measured simultaneously as to capture their values at the same temperatures and externally applied magnetic fields, making the determination of zT for magneto-thermoelectric phenomena increasingly challenging.

While zT values based on the Seebeck effect have been experimentally reported near 1[91–93] at room temperature and exceeding 2[94,95] at higher temperatures, $(zT)_{xxx}$, $(zT)_{xxz}$, and $(zT)_{xyz}$ are consistently at least an order of magnitude lower with maximal values observed below room temperature.[31,39,96] However, experimental work in magneto-thermoelectric materials majorly excludes reporting values of $(zT)_{xxx}$, $(zT)_{xxz}$, and $(zT)_{xyz}$, which are necessary within the community to determine the potential for device applications.

Device advantages and disadvantages of magneto-thermoelectrics

An advantage of the transverse thermoelectric conversion in conductors under magnetic fields and in magnetic materials with spontaneous magnetization is that it can occur in a wide variety of materials, without requiring special single crystals or hybrid structures. This versatility has led to a diversity of materials development for applications. The introduction of topological and layered materials has also led to new developments in condensed-matter physics. Because some materials that exhibit excellent transverse thermoelectric conversion properties require the application of a large external magnetic field, it is essential to develop transverse thermoelectric materials that exhibit large coercivity and remanent magnetization. Depending on target applications, the stray magnetic field generated by ferromagnetic materials may have a negative impact. With these points in mind, exploring new materials based on electronic structures[97] is necessary but not sufficient in developing transverse thermoelectric materials and devices using magnetic effects—nanostructure engineering to control magnetic properties is also important. The biggest issue in transverse thermoelectrics based on the magnetic effects is that its output power is still insufficient for thermal energy harvesting and electronic cooling applications. Thus, efforts are being made to solve this issue, for example, by hybridizing the transverse thermoelectric conversion phenomena based on the magnetic effects with those based on nonmagnetic effects, such as the off-diagonal Seebeck effect.[98,99] To bridge the gap between practical thermoelectric devices and magneto-thermoelectrics, it is necessary to optimize not only a thermopower

but also electrical and thermal conductivities. Based on the orthogonal relationship between charge and heat currents, anisotropic materials are suitable for optimizing the figure of merit for transverse thermoelectrics.[100]

Conclusion

Although the field of thermoelectrics has existed for over two centuries, recent discoveries in materials science have brought a resurgence of interest in magneto-thermoelectric effects. External magnetic fields can serve as the source of a skew force to enhance both longitudinal and transverse thermoelectric effects via the magneto-Seebeck and Nernst effects, respectively, while magnon excitations contribute to a longitudinal magnon-drag thermopower and a transverse SSE-induced ISHE. While magneto-thermoelectrics offer the opportunity to decouple the electric field and heat flux, presenting many advantages in device design, the figure of merit of magneto-thermoelectric materials still remains significantly lower than that of conventional thermoelectrics. Thus, effort in the field should further explore hybrid and nanostructures to bring magneto-thermoelectrics closer to device realization.

Acknowledgments

S.J.W. acknowledges support from the US Department of Energy, Office of Science, Office of Basic Energy Sciences Early Career Research Program (Award No. DE-SC0020154). T.K. acknowledges support from the Grant-in-Aid for Scientific Research (Grant No. JP24 K01326) from JSPS KAKENHI. B.S. acknowledges support from the Center for Emergent Materials, an NSF-funded MRSEC, under Grant No. DMR-2011876. K.U. was supported by JST ERATO "Magnetic Thermal Management Materials" (JPMJER2201) and the Grant-in-Aid for Scientific Research (S) (22H04965) from JSPS KAKENHI.

Author contributions

S.J.W.: Conceptualization (equal); visualization (equal); supervision (equal); writing—original draft (equal); writing—reviewing and editing (equal). T.K.: Writing—original draft (equal); writing—reviewing and editing (supporting). B.S.: Writing—original draft (equal); writing—reviewing and editing (supporting). K.U.: Conceptualization (equal); visualization (equal); writing—original draft (equal); writing—reviewing and editing (supporting).

Funding

Basic Energy Sciences, DE-SC0020154, S.W., JSPS KAKENHI, JP24K01326, T.K., Division of Materials Research, DMR-2011876, B.S., JST ERATO, JPMJER2201, K.U., JSPS KAKENHI, JP22H04965, K.U.

Conflict of interest

The authors declare no conflicts of interest.

Open Access

References

1. H.J. Goldsmid, *Introduction to Thermoelectricity* (Springer, Berlin, 2009)
2. J. He, T.M. Tritt, *Science* **357**, caak9997 (2017)
3. K. Uchida, S. Takahashi, K. Harii, J. Ieda, W. Koshibae, K. Ando, S. Maekawa, E. Saitoh, *Nature* **455**, 778 (2008)
4. S.-Y. Xu, I. Belopolski, N. Alidoust, M. Neupane, G. Bian, C. Zhang, R. Sankar, G. Chang, Z. Yuan, C.-C. Lee, S.-M. Huang, H. Zheng, J. Ma, D.S. Sanchez, B. Wang, A. Bansil, F. Chou, P.P. Shibayev, H. Lin, S. Jia, M.Z. Hasan, *Science* **7**, 613 (2015)
5. S.-Y. Xu, N. Alidoust, I. Belopolski, Z. Yuan, G. Bian, T.-R. Chang, H. Zheng, V.N. Strocov, D.S. Sanchez, G. Chang, C. Zhang, D. Mou, Y. Wu, L. Huang, C.-C. Lee, S.-M. Huang, B. Wang, A. Bansil, H.-T. Jeng, T. Neupert, A. Kaminski, H. Lin, S. Jia, M.Z. Hasan, *Nat. Phys.* **11**, 748 (2015)
6. B.Q. Lv, H.M. Weng, B.B. Fu, X.P. Wang, H. Miao, J. Ma, P. Richard, X.C. Huang, L.X. Zhao, G.F. Chen, Z. Fang, X. Dai, T. Qian, H. Ding, *Phys. Rev. X* **5**, 031013 (2015)
7. L.X. Yang, Z.K. Liu, Y. Sun, H. Peng, H.F. Yang, T. Zhang, B. Zhou, Y. Zhang, Y.F. Guo, M. Rahn, D. Prabhakaran, Z. Hussain, S.-K. Mo, C. Felser, B. Yan, Y.L. Chen, *Nat. Phys.* **11**, 728 (2015)
8. A.V. Ettingshausen, W. Nernst, *Ann. Phys. Chem.* **265**(10), 343 (1886)
9. J.P. Jan, *Solid State Physics* (Academic, New York, 1957), pp. 1–96
10. K. Uchida, S. Daimon, R. Iguchi, E. Saitoh, *Nature* **558**, 95 (2018)
11. K. Masuda, K. Uchida, R. Iguchi, Y. Miura, *Phys. Rev. B* **99**, 104406 (2019)
12. A. Sakai, Y.P. Mizuta, A.A. Nugroho, R. Sihombing, T. Koretsune, M.T. Suzuki, N. Takemori, R. Ishii, D. Nishio-Hamane, R. Arita, P. Goswami, *Nat. Phys.* **14**(11), 1119 (2018)
13. S.N. Guin, K. Manna, J. Noky, S.J. Watzman, C. Fu, N. Kumar, W. Schnelle, C. Shekhar, Y. Sun, J. Gooth, C. Felser, *NPG Asia Mater.* **11**, 16 (2019)
14. A. Sakai, S. Minami, T. Koretsune, T. Chen, T. Higo, Y. Wang, T. Nomoto, M. Hirayama, S. Miwa, D. Nishio-Hamane, F. Ishii, R. Arita, S. Nakatsuji, *Nature* **581**, 53 (2020)
15. T. Chen, S. Minami, A. Sakai, Y. Wang, Z. Feng, T. Nomoto, M. Hirayama, R. Ishii, T. Koretsune, R. Arita, S. Nakatsuji, *Sci. Adv.* **8**, eabk1480 (2022)
16. T. Kikkawa, E. Saitoh, *Annu. Rev. Condens. Matter Phys.* **14**, 129 (2023)
17. S.J. Watzman, R.A. Duine, Y. Tserkovnyak, S.R. Boona, H. Jin, A. Prakash, Y. Zheng, J.P. Heremans, *Phys. Rev. B* **94**, 144407 (2016)
18. N. Tsujii, A. Nishide, J. Hayakawa, T. Mori, *Sci. Adv.* **5**, eaat5935 (2019)
19. Y. Zheng, T. Lu, M.H. Md, M. Polash, N. Rasoulianboroujeni, M.E. Liu, Y. Manley, P.J. Deng, X.L. Sun, R.P. Chen, D. Hermann, J.P. Vashaee, HZhao Heremans, *Sci. Adv.* **5**, eaat9461 (2019)
20. K. Uchida, M. Ishida, T. Kikkawa, A. Kirihara, T. Murakami, E. Saitoh, *J. Phys. Condens. Matter* **26**, 343202 (2014)
21. K. Uchida, H. Adachi, T. Kikkawa, A. Kirihara, M. Ishida, S. Yorozu, S. Maekawa, E. Saitoh, *Proc. IEEE* **104**, 1946 (2016)
22. S. Maekawa, T. Kikkawa, H. Chudo, J. Ieda, E. Saitoh, *J. Appl. Phys.* **133**, 020902 (2023)
23. R. Lundgren, P. Laurell, G.A. Fiete, *Phys. Rev. B* **90**, 165115 (2014)
24. G. Sharma, P. Goswami, S. Tewari, *Phys. Rev. B* **93**, 035116 (2016)
25. T.M. McCormick, S.J. Watzman, J.P. Heremans, N. Trivedi, *Phys. Rev. B* **97**, 195152 (2018)
26. D. Xiao, Y. Yao, Z. Fang, Q. Niu, *Phys. Rev. Lett.* **97**, 026603 (2006)
27. D. Xiao, M.-C. Chang, Q. Niu, *Rev. Mod. Phys.* **82**, 1959 (2010)
28. T. Liang, J. Lin, Q. Gibson, T. Gao, M. Hirschberger, M. Liu, R.J. Cava, N.P. Ong, *Phys. Rev. Lett.* **118**, 136601 (2017)
29. S.J. Watzman, T.M. McCormick, C. Shekhar, S.-C. Wu, Y. Sun, A. Prakash, C. Felser, N. Trivedi, J.P. Heremans, *Phys. Rev. B* **97**, 161404(R) (2018)
30. C. Fu, S.N. Guin, S.J. Watzman, G. Li, E. Liu, N. Kumar, V. Suess, W. Schnelle, G. Auffermann, C. Shekhar, Y. Sun, J. Gooth, C. Felser, *Energy Environ. Sci.* **11**, 2813 (2018)

31. E.F. Scott, K.A. Schlaak, P. Chakraborty, C. Fu, S.N. Guin, S. Khodabakhsh, A.E. Paz y Puente, C. Felser, B. Skinner, S.J. Watzman, *Phys. Rev. B* **107**(11), 115108 (2023)
32. X. Feng, B. Skinner, *Phys. Rev. Mater.* **5**, 024202 (2021)
33. Y. Pan, B. He, T. Helm, D. Chen, W. Schnelle, C. Felser, *Nat. Commun.* **13**, 3909 (2022)
34. H. Yang, W. You, J. Wang, J. Huang, C. Xi, X. Xu, C. Cao, M. Tian, Z.-A. Dai, Y. Li, *Phys. Rev. Mater.* **4**, 024202 (2020)
35. S.N. Guin, P. Vir, Y. Zhang, N. Kumar, S.J. Watzman, C. Fu, E. Liu, K. Manna, W. Schnelle, J. Gooth, C. Shekhar, *Adv. Mater.* **31**(25), 1806622 (2019)
36. E. Liu, Y. Sun, N. Kumar, L. Muechler, A. Sun, L. Jiao, S.-Y. Yang, D. Liu, A. Liang, Q. Xu, J. Kroder, V. Suess, H. Bormann, C. Shekhar, Z. Wang, C. Xi, W. Wang, W. Schnelle, S. Wirth, Y. Chen, S.T.B. Goennenwein, C. Felser, *Nat. Phys.* **14**, 1125 (2018)
37. D. Xiong, Y. Jiang, K. Shi, A. Du, Y. Yao, Z. Guo, D. Zhu, K. Cao, S. Peng, W. Cai, D. Zhu, W. Zhao, *Fundam. Res.* **2**(4), 522 (2022)
38. S. Borisenko, D. Evtushinsky, Q. Gibson, A. Yaresko, K. Koepernik, T. Kim, M. Ali, J. van den Brink, M. Hoesch, A. Fedorov, E. Haubold, Y. Kushnirenko, I. Soldatov, R. Schäfer, R.J. Cava, *Nat. Commun.* **10**, 3424 (2019)
39. Y. Pan, C. Le, B. He, S.J. Watzman, M. Yao, J. Gooth, J.P. Heremans, Y. Sun, C. Felser, *Nat. Mater.* **21**, 203 (2022)
40. A. Miura, H. Sepehri-Amin, K. Masuda, H. Tsuchiura, Y. Miura, R. Iguchi, Y. Sakuraba, J. Shiomi, K. Hono, K. Uchida, *Appl. Phys. Lett.* **115**, 222403 (2019)
41. A. Miura, K. Masuda, T. Hirai, R. Iguchi, T. Seki, Y. Miura, H. Tsuchiura, K. Takanashi, K. Uchida, *Appl. Phys. Lett.* **117**, 082408 (2020)
42. F. Ando, T. Hirai, K. Uchida, *APL Energy* **2**, 016103 (2024)
43. W. Zhou, Y. Sakuraba, *Appl. Phys. Express* **13**, 043001 (2020)
44. T. Higo, Y. Li, K. Kondou, D. Qu, M. Ikhlas, R. Uesugi, D. Nishio-Hamane, C.L. Chien, Y.C. Otani, S. Nakatsuji, *Adv. Funct. Mater.* **31**, 2008971 (2021)
45. K. Uchida, W. Zhou, Y. Sakuraba, *Appl. Phys. Lett.* **118**, 140504 (2021)
46. S. Noguchi, K. Fujiwara, Y. Yanagi, M.-T. Suzuki, T. Hirai, T. Seki, K. Uchida, A. Tsukazaki, *Nat. Phys.* **20**, 254 (2024)
47. R. Modak, Y. Sakuraba, T. Hirai, T. Yagi, H. Sepehri-Amin, W. Zhou, H. Masuda, T. Seki, K. Takanashi, T. Ohkubo, K. Uchida, *Sci. Technol. Adv. Mater.* **23**, 767 (2022)
48. R. Gautam, T. Hirai, A. Alasli, H. Nagano, T. Ohkubo, K. Uchida, H. Sepehri-Amin, *Nat. Commun.* **15**, 2184 (2024)
49. W.-L. Lee, S. Watauchi, V.L. Miller, R.J. Cava, N.P. Ong, *Phys. Rev. Lett.* **93**, 226601 (2004)
50. M. Mizuguchi, S. Ohata, K. Uchida, E. Saitoh, K. Takanashi, *Appl. Phys. Express* **5**, 093002 (2012)
51. T. Seki, A. Miura, K. Uchida, T. Kubota, K. Takanashi, *Appl. Phys. Express* **12**, 023006 (2019)
52. M.A. Correa, A. Ferreira, A.L. Souza, J.M. Dantas Neto, F. Bohn, F. Vaz, G.V. Kurlyandskaya, *Sensors* (Basel) **23**(3), 1420 (2023)
53. R. Liu, L. Cai, T. Xu, J. Liu, Y. Cheng, W. Jiang, *Appl. Phys. Lett.* **122**, 022406 (2023)
54. S. J. Park, R. Modak, R. Gautam, A. Alasli, T. Hirai, F. Ando, H. Nagano, H. Sepehri-Amin, K. Uchida, Designing flexible hard magnetic materials for zero-magnetic-field operation of the anomalous Nernst effect (2024), Preprint, arXiv: 2412.08853
55. K. Fujiwara, Y. Kato, H. Abe, S. Noguchi, J. Shiogai, Y. Niwa, H. Kumigashira, Y. Motome, A. Tsukazaki, *Nat. Commun.* **14**, 3399 (2023)
56. K. Uchida, *Proc. Jpn. Acad. Ser. B* **97**(2), 69–88 (2021)
57. S. Seki, T. Ideue, M. Kubota, Y. Kozuka, R. Takagi, M. Nakamura, Y. Kaneko, M. Kawasaki, Y. Tokura, *Phys. Rev. Lett.* **115**, 266601 (2015)
58. S.M. Wu, W. Zhang, A. Kc, P. Borisov, J.E. Pearson, J.S. Jiang, D. Lederman, A. Hoffmann, A. Bhattacharya, *Phys. Rev. Lett.* **116**, 097204 (2016)
59. J. Li, C.B. Wilson, R. Cheng, M. Lohmann, M. Kavand, W. Yuan, M. Aldosary, N. Agladze, P. Wei, M.S. Sherwin, J. Shi, *Nature* **578**, 70 (2020)
60. W. Yuan, J. Li, J. Shi, *Appl. Phys. Lett.* **117**, 100501 (2020)
61. Y. Yamamoto, M. Ichioka, H. Adachi, *Phys. Rev. B* **105**, 104417 (2022)
62. P. Tang, G.E.W. Bauer, *Phys. Rev. Lett.* **133**, 036701 (2024)
63. N. Ito, T. Kikkawa, J. Barker, D. Hirobe, Y. Shiomi, E. Saitoh, *Phys. Rev. B* **100**, 060402(R) (2019)
64. W. Xing, L. Qiu, X. Wang, Y. Yao, Y. Ma, R. Cai, S. Jia, X.C. Xie, W. Han, *Phys. Rev. X* **9**, 011026 (2019)
65. G. Chen, S. Qi, J. Liu, D. Chen, J. Wang, S. Yan, Y. Zhang, S. Cao, M. Lu, S. Tian, K. Chen, P. Yu, Z. Liu, X.C. Xie, J. Xiao, R. Shindou, J.-H. Chen, *Nat. Commun.* **12**, 6279 (2021)
66. D.K. de Wal, M. Zohaib, B.J. van Wees, *Phys. Rev. B* **110**, 174440 (2024)
67. T. Liu, J. Peiro, D.K. de Wal, J.C. Leutenantsmeyer, M.H.D. Guimarães, B.J. van Wees, *Phys. Rev. B* **101**, 205407 (2020)
68. S.-K. Lee, W.-Y. Lee, T. Kikkawa, C.T. Le, M.-S. Kang, G.-S. Kim, A.D. Nguyen, Y.S. Kim, N.-W. Park, E. Saitoh, *Adv. Funct. Mater.* **30**, 2003192 (2020)
69. M.-H. Phan, M.T. Trinh, T. Eggers, V. Kalappattil, K. Uchida, L.M. Woods, M. Terrones, *Appl. Phys. Lett.* **119**, 250501 (2021)
70. F.J. Blatt, D.J. Flood, V. Rowe, P.A. Schroeder, J.E. Cox, *Phys. Rev. Lett.* **18**, 395 (1967)
71. C. Kittel, *Quantum Theory of Solids* (Wiley, New York, 1963)
72. B. He, C. Sahin, S.R. Boona, B.C. Sales, Y. Pan, C. Felser, M.E. Flatte, J.P. Heremans, *Joule* **5**, 3057 (2021)
73. G.N. Grannemann, L. Berger, *Phys. Rev. B* **13**, 2072 (1976)
74. J.M. Ziman, *Electrons and Phonons* (Clarendon Press, Oxford, 1960)
75. M.E. Lucassen, C.H. Wong, R.A. Duine, Y. Tserkovnyak, *Appl. Phys. Lett.* **99**, 262506 (2011)
76. B. Flebus, R.A. Duine, Y. Tserkovnyak, *Europhys. Lett.* **115**, 57004 (2016)
77. E.H. Putley, *The Hall Effect and Related Phenomena*, 1st ed. (Butterworths, London, 1960)
78. I. Sodemann, L. Fu, *Phys. Rev. Lett.* **115**, 216806 (2015)
79. Q. Ma, S.Y. Xu, H. Shen, D. MacNeill, V. Fatemi, T.R. Chang, A.M. Mier Valdivia, S. Wu, Z. Du, C.H. Hsu, S. Fang, *Nature* **565**(7739), 337 (2019)
80. K. Kang, T. Li, E. Sohn, J. Shan, K.F. Mak, *Nat. Mater.* **18**, 324 (2019)
81. J.-W. Chen, T. Ishii, S. Pu, N. Yamamoto, *Phys. Rev. D* **93**, 125023 (2016)
82. R. Nakai, N. Nagaosa, *Phys. Rev. B* **99**, 115201 (2019)
83. C. Zeng, S. Nandy, S. Tewari, *Phys. Rev. Res.* **2**, 032066 (2020)
84. X. Yang, B. Skinner. Nonlinear thermoelectric effects as a means to probe quantum geometry (2025). Preprint, https://arxiv.org/pdf/2505.00086
85. C. Zeng, S. Nandy, A. Taraphder, S. Tewari, *Phys. Rev. B* **100**, 245102 (2019)
86. X.-Q. Yu, Z.-G. Zhu, J.-S. You, T. Low, G. Su, *Phys. Rev. B* **99**, 201410 (2019)
87. Y. Zhang, Y. Sun, B. Yan, *Phys. Rev. B* **97**, 041101(R) (2018)
88. C. Zeng, S. Nandy, S. Tewari, *Phys. Rev. B* **103**, 245119 (2021)
89. H. Varshney, A. Agarwal, Intrinsic nonlinear Nernst and Seebeck effect (2024), Preprint, arXiv:2409.11108
90. H. Arisawa, Y. Fujimoto, T. Kikkawa, E. Saitoh, *Nat. Commun.* **15**, 6912 (2024)
91. S.I. Kim, K.H. Lee, H.A. Mun, H.S. Kim, S.W. Hwang, J.W. Roh, D.J. Yang, W.H. Shin, X.S. Li, Y.H. Lee, G.J. Snyder, S.W. Kim, *Science* **348**, 109 (2015)
92. D.-Y. Chung, T.P. Hogan, M. Rocci-Lane, P. Brazis, J.R. Ireland, C.R. Kannewurf, M. Bastea, C. Uher, M.G. Kanatzidis, *J. Am. Chem. Soc.* **126**, 6414 (2004)
93. A.F. May, J.-P. Fleurial, G.J. Snyder, *Phys. Rev. B* **78**, 125205 (2008)
94. K.F. Hsu, S. Loo, F. Guo, W. Chen, J.S. Dyck, C. Uher, T. Hogan, E.K. Polychroniadis, M.G. Kanatzidis, *Science* **303**, 818 (2004)
95. K. Biswas, J. He, I.D. Blum, C.-I. Wu, T.P. Hogan, D. Seidman, V.P. Dravid, M.G. Kanatzidis, *Nature* **489**, 414 (2012)
96. M.S. Akhanda, K.A. Schlaak, E.F. Scott, M.N.A. Taj, S.J. Watzman, M. Zebarjadi, *J. Appl. Phys.* **135**, 240901 (2024)
97. S. Liu, M. Chen, C. Fu, T. Zhu, *Adv. Phys. Res.* **2**(9), 2300015 (2023)
98. K. Uchida, T. Hirai, F. Ando, H. Sepehri-Amin, *Adv. Energy Mater.* **14**, 2302375 (2024)
99. T. Hirai, F. Ando, H. Sepehri-Amin, K. Uchida, *Nat. Commun.* **15**, 9643 (2024)
100. K. Uchida, *Nat. Mater.* **21**, 136 (2022) □

Sarah J. Watzman is an associate professor in the Department of Mechanical and Materials Engineering at the University of Cincinnati. She received her PhD degree at The Ohio State University in 2018. Her research focuses on understanding the interplay of thermal, electrical, and magnetic transport as a way to inform design of more energy-efficient solid-state devices, with a particular interest in topological materials. Watzman can be reached by email at watzmasj@ucmail.uc.edu.

Takashi Kikkawa has been a team leader at the Advanced Science Research Center, Japan Atomic Energy Agency, since 2024. Previously, he was an assistant professor at Tohoku University and The University of Tokyo, Japan, from 2018 to 2024. He received his PhD degree from Tohoku University, Japan, in 2018. His research interests include spin(calori)tronics, condensed-matter physics, and energy conversion. Kikkawa can be reached by email at kikkawa.takashi@jaea.go.jp.

Brian Skinner is an associate professor of physics at The Ohio State University. He received his PhD degree from the University of Minnesota in 2011. He held postdoctoral positions at Argonne National Laboratory and the Massachusetts Institute of Technology before joining the faculty at Ohio State in 2020. He has widespread interests relating to dynamical and transport phenomena in many-body quantum systems. Skinner can be reached by email at skinner.352@osu.edu.

Ken-ichi Uchida has been a Distinguished Group Leader of the Research Center for Magnetic and Spintronic Materials at the National Institute for Materials Science (NIMS), Japan, since 2023 and professor of the Graduate School of Frontier Science at The University of Tokyo, Japan, since 2024. Previously, he was an assistant/associate professor from 2012 to 2016 at Tohoku University, Japan, and group leader at NIMS. He has been leading the JST ERATO project and working mainly on spintronics and thermoelectrics. Uchida can be reached by email at UCHIDA.Kenichi@nims.go.jp.